A Data-Driven-Based Wide-Area Protection Scheme for Fault Detection Using the Limited Measurements

Sirwan Shazdeh, Qobad Shafiee and Hassan Bevrani
Smart/Micro Grids Research Center, University of Kurdistan, Pasdaran Boulevard, PO Box 416, Sanandaj, Iran
s.shazdeh@uok.ac.ir, q.shafiee@uok.ac.ir, h.bevrani@uok.ac.ir

Keywords: Fault Detection, Wide-Area Protection, Data-Driven Scheme, Intelligent Electronic Devices (IEDs), Microgrid (MG).

Abstract: This paper presents a novel and efficient approach for wide-area fault detection in microgrids, utilizing data-driven techniques based on voltage and current measurements. The proposed method offers both high speed and accuracy in detecting faults. The methodology consists of three key steps that collectively form a comprehensive protection scheme. Initially, the current trajectories obtained from the measurements are analyzed to determine the fault condition. This initial indicator serves as a valuable starting point for fault detection. In the second step, the impedance of the lines, including the considered area, is calculated for the fault detection. The change of the calculated impedances implies for the fault occurrence activating the third step. In the final step, an iterative process is followed to identify the faulted line. The proposed method provides a faster and more reliable fault detection mechanism, allowing for rapid response and mitigation of potential disruptions. The efficacy of the proposed method is validated on an 11-bus microgrid. The simulation investigations are conducted in MATLAB\SIMULINK environment.

1 INTRODUCTION

Due to the escalating concerns of global warming, economic and power loss issues, and the growing demand for electricity, the utilization of renewable energy sources (RESs) as micro-sources in close proximity to the load has witnessed a significant surge at the distribution level. The integration of electrical loads and distributed generations (DGs) forms microgrids (MGs) that operate in both grid-connected and islanded modes [1]. However, despite the evident advantages of MGs, they face a multitude of technical problems and challenges, particularly in the areas of control, operation, and protection [2], [3]. Notably, this paper focuses on the protection challenges within MGs.

The reliable and secure operation of protection systems in MGs is severely affected by various factors, including different short circuit levels in grid-connected and islanded modes, limited current capacity of inverter-based DGs due to insulation issues, the intermittent nature of RESs, and continuous changes in the grid topology [4]. These factors collectively undermine the efficacy of protection systems, and any unplanned disconnection of equipment in MGs, resulting from inadequate performance of protection systems, can lead to unstable conditions due to the limited capacity of DGs.

Consequently, extensive research efforts have been devoted to addressing these challenges [5, 6]. Various adaptive-based protection approaches, ranging from decentralized to centralized actions, have been introduced to determine suitable settings for protection functions [5]. Furthermore, significant contributions have been made to enhance vulnerable protection systems such as distance, overcurrent, and differential functions. Notable advancements in this area can be found in prior works, which build upon the conventional principles of protection devices [7 - 11]. However, challenges persist, including the need for information from the opposite end of the line, communication vulnerabilities, the complexity of setting determination in the face of frequent topology changes, and issues related to the reliability and functionality of protection devices.

In addition to conventional protection-based approaches, several signal-processing-based schemes have been employed to extract relevant features for

accurate fault detection [12]. However, the correct performance of signal-processing-based approaches is hindered by challenges such as intricate threshold determination, susceptibility to measurement errors, and the complex operational conditions of MGs.

Given the significant advancements in artificial intelligence (AI) techniques, AI-based approaches have garnered increased attention for fault detection and identification, particularly in light of the sophisticated and unpredictable conditions encountered in MG operations [13]. For instance, a fault detection method based on support vector machines has been proposed in [14]. Furthermore, the combination of AI-based approaches with knowledge-based schemes has been introduced to enhance the accuracy of fault detection and identification in MGs. An example of this is the integration of deep neural network techniques with Discrete Wavelet Transform, as presented in [15], to overcome fault detection challenges. Another approach in [16] incorporates a decision tree (DT)-based method with fuzzy logic, serving as a knowledge-based scheme, to facilitate reliable decision-making. However, it is worth noting that these approaches exhibit high-performance capabilities but necessitate extensive and comprehensive training data to effectively address the complexity and unprecedented conditions encountered in MG operations.

Another interesting protection strategy belongs to the multi-agent systems using various agents. For instance, a multi-agent-based protection system is proposed in [17] using the current angle of both sides of a line. Determination of the required criteria and the need for extensive data from different points make the multi-agent-based methods more expensive and complex.

In addition, with the advent of advanced measurement, computation, and communication technologies, the integration of these devices into MG protection systems has become widespread. While local protection functions remain essential due to their swift performance and lack of communication failure risks, the implementation of a wide-area structure becomes imperative in order to gather data from multiple points and make supervisory and back-up decisions, thereby enhancing the reliability and security of protection systems in MGs.

In this regard, based on the data acquired from phasor measurement units (PMUs) in MGs, different protection applications are managed [18]. A coordinated protection and control system is achieved in [19] using the frequency data from PMUs. Moreover, a supervisory level is produced to enhance the security and selectivity of the local protection systems by authors in [20]. In another approach, the PMU data is used for the MG islanding detection and provides a corrective strategy for the misoperation prevention of the protection systems.

It is noteworthy that wide-area protection applications are accessible concerning the speed, simplicity, security of the communication systems, and accuracy of the approaches.

Accordingly, this paper proposes a simple, accurate, and fast wide-area backup protection for fault detection and identification using the intelligent electronic devices (IEDs), installed in limited locations. More precisely, the proposed method uses data from IEDs without the need for line parameter information. According to the proposed method, each non-IED bus is surrounded by IED buses through the distribution lines. After the fault detection step, the faulted line is identified without the need for information related to the branches connected to the non-IED bus, such as lines and load information.

The proposed method does not need for criterion definition for fault detection. Indeed, it provides a model-free approach and is robust against events such as load-change and line outage.

Accordingly, the contributions and features of the proposed method are listed as follows.

- Presentation of an approach for fault detection without the need for line parameters and load information;
- Determination of the faulted line without the need for line and load information;
- Determination of the line parameters during the load-increasing event;
- Prevention of the misoperation protection during non-fault conditions.

The rest of the paper is organized as follows. Section II explains the details of the proposed method. Simulation results verify the proposed method's performance in section III. Finally, the last section belong to the conclusion and discussion about the performance of the proposed method.

2 METHODOLOGY

A novel numerical measurement-based scheme is proposed in this study, utilizing voltage and current data obtained from IEDs to establish an efficient and dependable approach for fault detection and identification. The following sections elaborate on the detailed process of the proposed method.

2.1 IED Placement Strategy

The installation of IEDs follows a strategic approach wherein IED buses surround each non-IED bus through the distributed lines. This placement strategy is graphically represented in Figure 1. According to this strategy, each IED bus is connected to at least one non-IED bus.

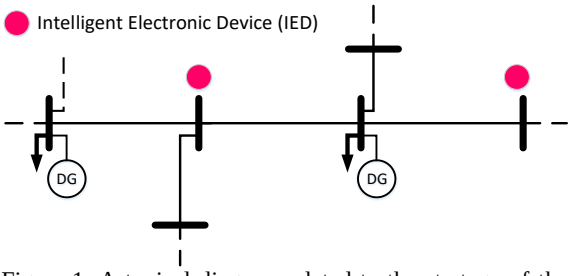

Figure 1: A typical diagram related to the strategy of the IEDs placement.

2.2 Fault Detection Approach

When a fault occurs at location f, the voltage at the fault location drops to zero, as depicted in Figure 2a. Consequently, the current flowing through the p-bus experiences a sudden increase due to the sharp voltage drop from the normal condition. To provide further clarity, the current drawn from the p-bus is calculated for both normal and fault conditions based on the Kirchhoff's Voltage Law (KVL), as outlined (1):

$$I_p = \frac{V_p - V_q}{Z_{pq}}, \qquad I_{p-f} = \frac{V_p - V_f}{Z_{pf}}. \tag{1}$$

where V_p, V_q, V_f, Z_{pq}, and Z_{pf} stand for the voltage of p, q, and fault location, the line impedance between p and q buses, and the line impedance between p and f location, respectively.

This observed increase in current during fault occurrence serves as an initial indicator for fault detection. It is important to note that this indication may also arise in similar events such as load-increasing and disconnection of DGs from non-IED buses. However, this rule can effectively differentiate faults from other events like line outages. During a line outage, the current in the associated line becomes zero. To distinguish fault occurrences from similar events like load-increasing and DG disconnection, the KVL is applied to the electrical circuit, as demonstrated in Figure 2b:

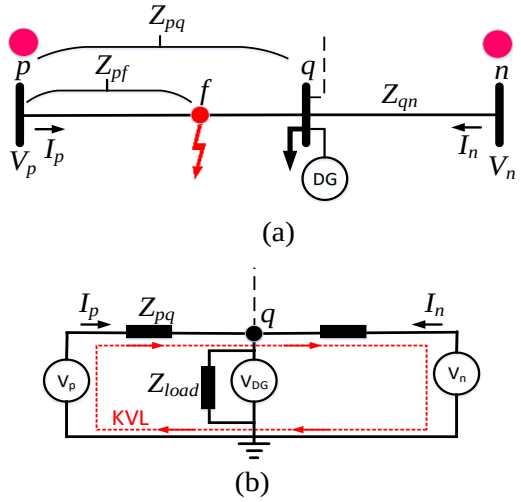

Figure 2: Schematic of the considered area: a) during the fault occurrence, b) equivalent circuit in normal condition.

$$V_p = Z_{pq} I_p + V_q - Z_{qn} I_n + V_n, \tag{2}$$

where Z_{qn}, I_n, and V_n are known as the line impedance between n and q buses, current flowing the line between n and q buses, and n-bus voltage, respectively. By dividing (2) to I_p, one can write:

$$\frac{V_p}{I_p} = Z_{pq} + \frac{V_q}{I_p} - Z_{qn}\frac{I_n}{I_p} + \frac{V_n}{I_p}. \tag{3}$$

It can be observed that the voltage and current values of the p and q buses are accessible through the installed IEDs, and (3) can be rearranged as follows.

$$Z_{pq} + \frac{V_q}{I_p} - Z_{qn}\frac{I_n}{I_p} + \frac{V_n}{I_p} - \frac{V_p}{I_p} = 0. \tag{4}$$

According to (4), there is an equation with two unknown variables, Z_{pq} and Z_{qn}.

In this step, when there is no fault or line outage, the values of Z_{pq} and Z_{qn} remain constant. Consequently, a numerical approach is employed to solve (4) and determine the unknown variables. To achieve this, two sequential samples of both voltage and current measurements are utilized, as follows (5):

$$Z_{pq} + \frac{V_q(h-1)}{I_p(h-1)} - Z_{qn}\frac{I_n(h-1)}{I_p(h-1)} + \frac{V_n(h-1)}{I_p(h-1)} - \frac{V_p(h-1)}{I_p(h-1)} = 0,$$
$$Z_{pq} + \frac{V_q(h)}{I_p(h)} - Z_{qn}\frac{I_n(h)}{I_p(h)} + \frac{V_n(h)}{I_p(h)} - \frac{V_p(h)}{I_p(h)} = 0, \tag{5}$$

where h is the sample number of measurements.

Therefore, at each instance, there are two equations with two unknown variables. Based on the equations derived from the measurement samples, the values of Z_{pq} and Z_{qn} are calculated using the most

recent and previous samples. If the obtained values for these variables remain constant, it indicates the absence of faults on the considered lines for the given event. Conversely, if the values change, it signifies that one of the considered lines within the studied area has experienced a fault.

2.3 Fault Localization

Once a fault is detected, the next crucial step involves determining the specific location of the faulted line. Let us assume that the fault occurs at location f in Figure 3a, characterized by a resistance value of R. In Figure 3a, the variable x represents the ratio of the fault distance to the line length. To facilitate this process, the circuit's T-structure model is transformed into a Π model, as illustrated in Figure 3b.

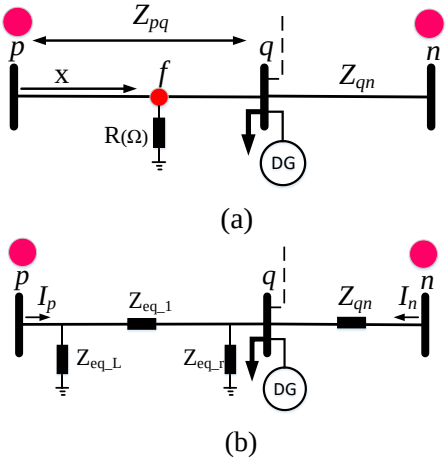

Figure 3: Diagram of the faulted area, a) location and resistance of the fault, b) transformed form of the faulted line.

By following process for the transformation of the delta connection to star connection based on the Kirchhoff's current Law (KCL) and KVL, the relationship is expressed as (6):

$$\begin{aligned} Z_{eq1} &= \frac{Z_1Z_2+Z_2R+Z_1R}{R}, \\ Z_{eq\_r} &= \frac{Z_1Z_2+Z_2R+Z_1R}{Z_1}, \\ Z_{eq\_l} &= \frac{Z_1Z_2+Z_2R+Z_1R}{Z_2}. \end{aligned} \tag{6}$$

Where:

$$\begin{aligned} Z_1 &= xZ_{pq}, \\ Z_2 &= (1-x)Z_{pq}. \end{aligned} \tag{7}$$

Applying the KVL and KCL to the circuit depicted in Figure 3b, we obtain (8) as follows:

$$V_n = Z_{nq}I_n - Z_{eq1}(I_p - \frac{V_p}{Z_{eq\_l}}) + V_p. \tag{8}$$

By simplification and dividing (8) to I_n, one can find:

$$\frac{V_n}{I_n} - Z_{nq} + Z_{pq}\frac{I_p}{I_n} - \frac{V_p}{I_n} = \frac{(1-x)Z_{pq}}{R}\frac{V_p}{I_n} - \frac{x(1-x){Z_{pq}}^2}{R}\frac{I_p}{I_n}. \tag{9}$$

In (9), we have two unknown variables, x and R. To solve this problem, a repetitive process is employed. For instance, assuming a numeric value for x, we calculate the corresponding value for R based on eq (9). If the obtained value for R is positive for one iteration and negative for the subsequent iteration of x, this pair of x and R is considered as the fault location and resistance on the relevant line. Otherwise, if the R is not a rational value, it indicates that the adjacent line has been subjected to the fault.

Figure 4 shows the overall flowchart of the proposed method for fault detection and identification.

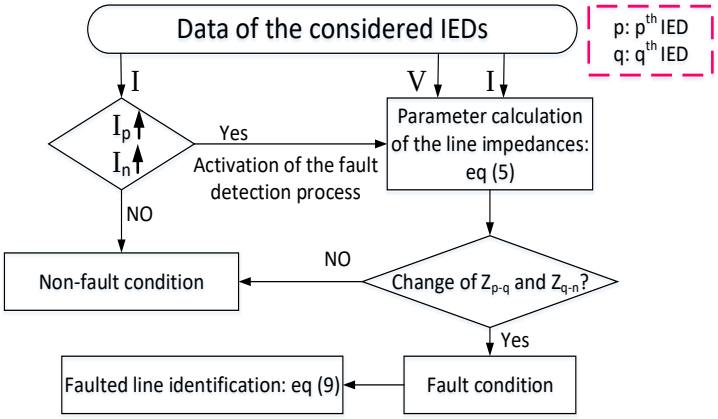

Figure 4: Flowchart of the proposed method for fault detection and faulted line determination.

3 SIMULATION AND RESULTS

In this section, simulation tests were performed to validate the proposed method within the MATLAB/SIMULINK environment. To this end, an 11-bus MG [21] was chosen as an autonomous test system to introduce the necessary disturbances. Figure 5 displays a schematic representation of the 11-bus test case.

For the initial evaluation, a three-phase fault with a resistance of R=0.001 Ω was applied to the middle of line 8-7, from t=0.1 s to t=0.2 s. In this scenario, the currents flowing through both lines, 8-7 and 7-3, increase at the moment of fault occurrence. The current trends are depicted in Figure 6a, indicating the activation of the fault detection process. The proposed approach of impedance calculation was employed in this regard. Figure 6b illustrates the results of the obtained $Z_{8\text{-}7}$ and $Z_{7\text{-}3}$ based on the proposed method. Notably, the actual impedance values are $Z_{8-7} = (0.0261 + 0.0025i)$ and $Z_{7-3} = (0.066 + 0.0128i)$. Notably, i stands for imaginary part of the complex numbers which is equal to $\sqrt{-1}$.

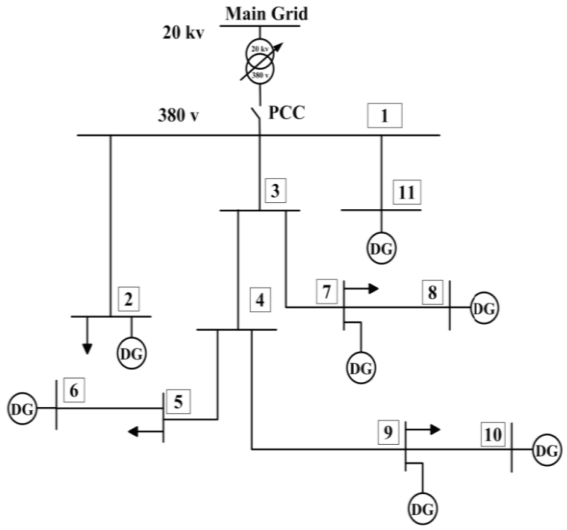

Figure 5: Single diagram of the 11-bus case study.

The obtained results demonstrate that the calculated impedances undergo changes during the fault occurrence, with magnitudes comparable to the actual impedance values. Following fault clearance, the calculated impedances return to their pre-fault conditions.

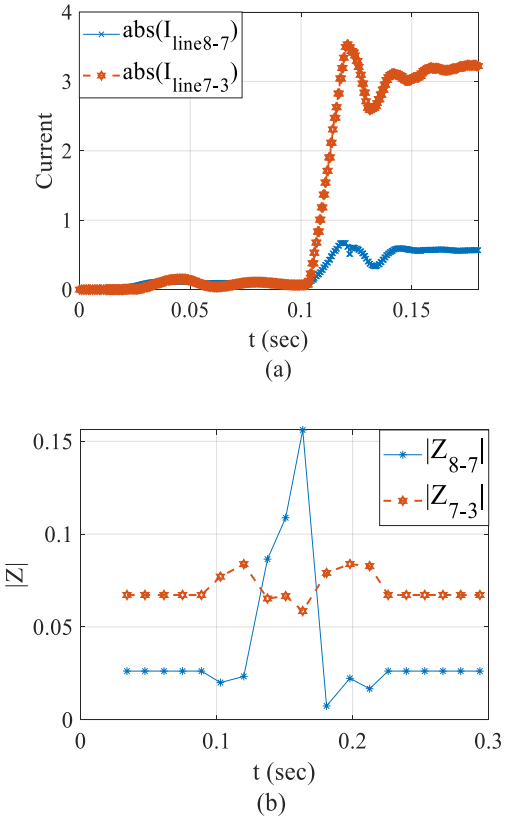

Figure 6: Simulation results for fault on line 8-7 with R=0.001 Ω: a) current values for both considered lines, b) calculated impedance.

To determine the faulted line, an iterative process involving line 8-7 and line 7-3 is initiated. Based on the obtained values of R, as indicated in Table 1, assuming the fault occurred on line 8-7, the calculated R values for different iterations of x are found to have positive real values. Specifically, the real part of the calculated R confirms that the fault was applied on line 8-7 with low resistance, and the fault location is likely to be within the range of x=0.1 to x=0.7. Conversely, assuming the fault occurred on line 7-3, the obtained R values, presented in Table 2, are negative and irrational.

Table 1: Calculated values of R for different x assuming the fault occurrence on line 8-7.

X	R
0.1	0.0043 - 0.0005i
0.3	0.0023 - 0.0003i
0.5	0.0010 - 0.0001i
0.7	0.0002 - 0.0001i
0.9	-0.0001 - 0.0000i

Assuming the fault occurrence on line 7-3, the calculated of R values for different fault distances (different x) will be negative, as shown in Table 2, indicating the false assumption of the fault location.

Table 2: Calculated values of R for different x assuming the fault occurrence on line 7-3.

x	R
0.1	-0.6881 - 0.7459i
0.3	-0.5043 - 0.5702i
0.5	-0.3381 - 0.4002i
0.7	-0.1896 - 0.2359i
0.9	-0.0588 - 0.0772i

To demonstrate the effect of load increase on the proposed method, the load connected to bus 7 was doubled compared to its normal condition. Despite exhibiting a similar trend to the currents with the fault conditions, the calculated impedance, as shown in Figure 7, remains unchanged. This observation indicates a non-fault condition.

In another scenario, the DG connected to bus 7 was disconnected from t=0.1 s to t=0.2 s. The results indicate that the calculated impedances for $Z_{8\text{-}7}$ and $Z_{7\text{-}3}$ remain constant, as depicted in Figure 8. Notably, during this condition, conventional protection systems may make incorrect decisions due to the increased current. However, the proposed method can easily discriminate between fault and non-fault conditions.

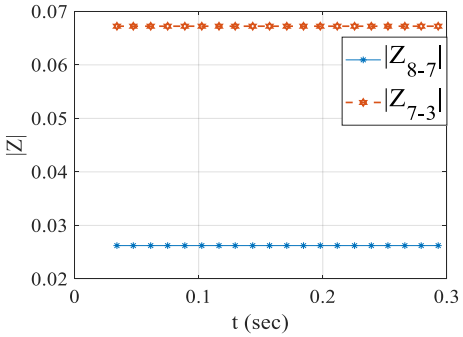

Figure 7: Absolute value of the calculated impedance for the load-increasing from t=0.1 s to t=0.2 s.

Another challenging event for conventional protection systems is line outage. To evaluate the performance of the proposed method, line 8-7 was temporarily removed from the system from t=0.1 s for a duration of 0.1 s. As shown in Figure 9, the line current becomes zero, while the magnitude of the calculated impedance parameters changes significantly, indicating a line outage. The decrease in current and high values of the impedance parameters imply a non-fault condition.

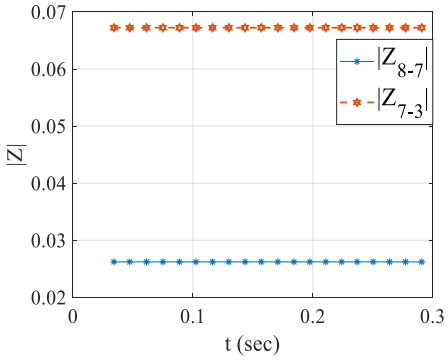

Figure 8: Absolute value of the calculated impedance for DG outage from bus 7 from t=0.1 s to t=0.2 s.

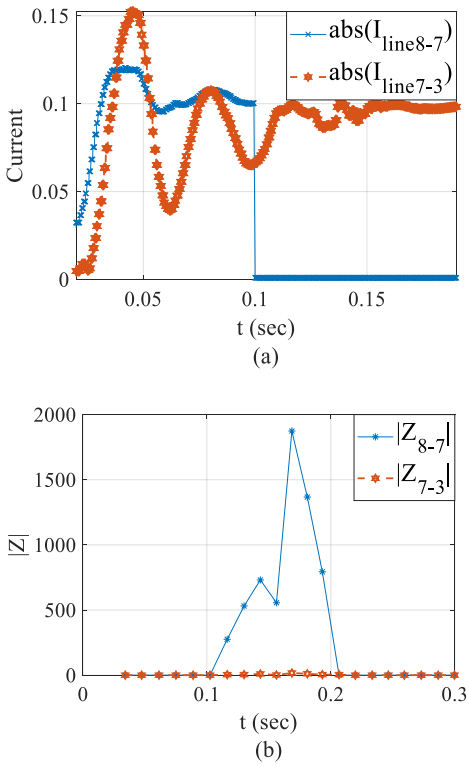

Figure 9: Results in response to line 8-7 outage at t=0.1 s to t=0.2 s, a) current trajectory of the considered lines, b) absolute values of the calculated impedances.

For further investigations, a three-phase fault with R=50 Ω was applied to the middle of line 8-7 at t=0.1 s, lasting for 0.1 s. The calculated impedances, as shown in Figure 10, confirm the occurrence of a fault at t=0.1 s, based on the changing values of the calculated parameters.

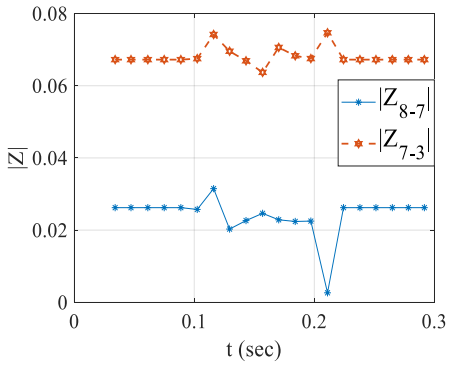

Figure 10: Absolute values of the calculated impedances for fault on the line 8-7 with R=50 Ω.

In another scenario, line 9-4 was subjected to a three-phase fault with R=10 Ω. The fault was located at a distance 0.2 times the line length from bus 9 and lasted for 0.1 s from t=0.1 s. The calculated impedances, $Z_{9\text{-}4}$ and $Z_{5\text{-}4}$, representing the considered lines impedances, are presented in Figure 11. The obtained results demonstrate that the calculated parameters change simultaneously with the fault occurrence, starting from t=0.1 s.

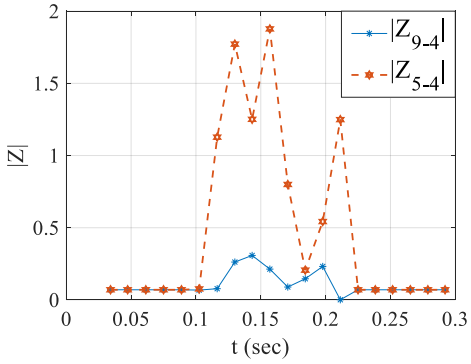

Figure 11: Absolute values of the calculated impedances for the fault on the line 9-4 from t=0.1 s to t=0.2 s with R=10 Ω.

Table 3 displays the obtained parameters related to the fault resistance for x=0.2, assuming the fault occurred on line 9-4. The positive value confirms the assumption of fault location. Conversely, assuming the fault occurred on line 5-4, the obtained R values are not acceptable. According to the obtained values for R assuming the fault occurrence on lines 9-4 and 5-4, respectively, in Table 3, the actual fault location is determined based on the rational and positive R value when line 9-4 has been subjected to the fault, especially for x=0.2.

Table 3. Values of R for x=0.2 assuming fault occurrence on the lines 9-4 and 5-4.

Assuming the fault on the line 9-4	
x	R
0.2	9.8910 + 0.3160i
Assuming fault on the line 5-4	
x	R
0.2	-9.9486 - 0.3086i

The effect of the applied fault on line 9-4 was investigated by analyzing the calculated impedances of $Z_{5\text{-}4}$ and $Z_{3\text{-}4}$, representing the main lines impedances. The results, as depicted in Figure 12, indicate that the values of $Z_{5\text{-}4}$ and $Z_{3\text{-}4}$ remain constant throughout the fault occurrence on line 9-4, which is connected to bus 4. This observation verifies that faults occurring on lines outside the considered area have no effect on the calculated impedances, and they remain unchanged.

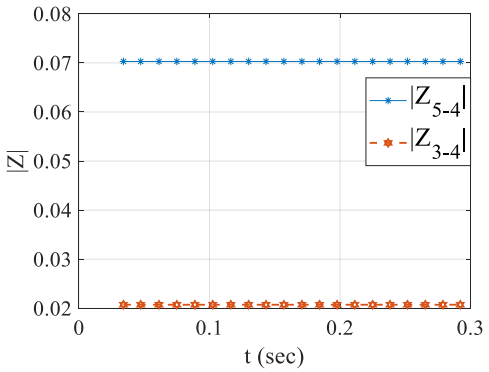

Figure 12: Absolute of calculated impedances related to $Z_{5\text{-}4}$ and $Z_{3\text{-}4}$ during the fault on the line 9-4 at t=0.1 s to t=0.2 s.

In this work, the reporting rate of IEDs was set to 60 samples per second. Consequently, the decision-making time for fault detection, assuming two samples for each decision, was determined to be 34 ms. This fast decision-making time demonstrates the efficient performance of the proposed method.

4 CONCLUSIONS

This paper presents an innovative data-driven wide-area backup protection approach for fault detection. The proposed method offers a reliable solution for detecting fault conditions along the primary route of the lines between the two IED-buses, without relying on detailed information about the lines, load, DGs, or the equipment connected to non-IED-buses. Through a repetitive approach, the faulted line is accurately identified following fault detection.

The results obtained from this study reveal that the correct performance of the proposed method remains unaffected by non-fault disturbances. Furthermore, the efficacy of the approach remains intact even when faults occur outside the designated area of interest. These findings serve as concrete evidence, validating the speed of the proposed method, which requires a maximum of two sequential calculated samples to arrive at a suitable decision.

It is important to note that the potential impact of measurement errors on the performance of the proposed method has not been taken into consideration. Additionally, despite the limited number of measurements employed in this paper, future research endeavors will explore an evolved method that relies on a reduced number of measurements, aiming to enhance fault detection capabilities.

REFERENCES

[1] M. Farrokhabadi et al., "Microgrid Stability Definitions, Analysis, and Examples," IEEE Trans. Power Syst., vol. 35, no. 1, pp. 13-29, 2020, doi: 10.1109/TPWRS.2019.2925703.

[2] W.M. Hamanah, M.I. Hossain, M. Shafiullah, and M.A. Abido, "AC Microgrid Protection Schemes: A Comprehensive Review," IEEE Access, vol. 11, pp. 76842-76868, 2023, doi: 10.1109/ACCESS.2023.3298306.

[3] G.S. Dua, B. Tyagi, and V. Kumar, "Fault Detection Technique for Distribution Networks and Microgrids Using Synchrophasor Data," IEEE Trans. Ind. Appl., pp. 1-14, 2023, doi: 10.1109/TIA.2023.3305362.

[4] M.W. Altaf, M.T. Arif, S.N. Islam, and M.E. Haque, "Microgrid Protection Challenges and Mitigation Approaches–A Comprehensive Review," IEEE Access, vol. 10, pp. 38895-38922, 2022, doi: 10.1109/ACCESS.2022.3165011.

[5] P.H.A. Barra, D.V. Coury, and R.A. S. Fernandes, "A survey on adaptive protection of microgrids and distribution systems with distributed generators," Renew. Sustain. Energy Rev., vol. 118, September 2019, p. 109524, 2020, doi: 10.1016/j.rser.2019.109524.

[6] A. Dagar, P. Gupta, and V. Niranjan, "Microgrid protection: A comprehensive review," Renew. Sustain. Energy Rev., vol. 149, no. June, p. 111401, 2021, doi: 10.1016/j.rser.2021.111401.

[7] S. Mirsaeidi, D. Mat Said, M.W. Mustafa, and M. Hafiz Habibuddin, "A protection strategy for micro-grids based on positive-sequence component," IET Renew. Power Gener., vol. 9, no. 6, pp. 600–609, 2015, doi: https://doi.org/10.1049/iet-rpg.2014.0255.

[8] K.A. Saleh and A. Mehrizi-Sani, "Harmonic Directional Overcurrent Relay For Islanded Microgrids With Inverter-Based DGs," IEEE Syst. J., vol. 15, no. 2, pp. 2720-2731, 2021, doi: 10.1109/JSYST.2020.2980274.

[9] A.D. Bebars, A.A. Eladl, G.M. Abdulsalam, and E.A. Badran, "Internal electrical fault detection techniques in DFIG-based wind turbines: a review," Prot. Control Mod. Power Syst., vol. 7, no. 1, p. 18, 2022, doi: 10.1186/s41601-022-00236-z.

[10] M.N. Alam, "Overcurrent protection of AC microgrids using mixed characteristic curves of relays," Comput. Electr. Eng., vol. 74, pp. 74-88, 2019, doi: https://doi.org/10.1016/j.compeleceng.2019.01.003.

[11] P.T. Manditereza and R.C. Bansal, "Protection of microgrids using voltage-based power differential and sensitivity analysis," Int. J. Electr. Power Energy Syst., vol. 118, p. 105756, 2020, doi: https://doi.org/10.1016/j.ijepes.2019.105756.

[12] A.N. Sheta, G.M. Abdulsalam, B.E. Sedhom, and A.A. Eladl, Comparative framework for AC-microgrid protection schemes: challenges, solutions, real applications, and future trends, vol. 8, no. 1. Springer Nature Singapore, 2023. doi: 10.1186/s41601-023-00296-9.

[13] N. Hussain, M. Nasir, J.C. Vasquez, and J. M. Guerrero, "Recent developments and challenges on AC microgrids fault detection and protection systems-a review," Energies, vol. 13, no. 9, 2020, doi: 10.3390/en13092149.

[14] J. C. Vasquez, "Adaptive protection combined with machine learning for microgrids," IET Gener. Transm. Distrib., vol. 13, no. 6, pp. 770-779(9), March 2019, [Online]. Available: https://digital-library.theiet.org/content/journals/10.1049/iet-gtd.2018.6230

[15] J.J.Q. Yu, Y. Hou, A.Y.S. Lam, and V.O.K. Li, "Intelligent Fault Detection Scheme for Microgrids With Wavelet-Based Deep Neural Networks," IEEE Trans. Smart Grid, vol. 10, no. 2, pp. 1694-1703, 2019, doi: 10.1109/TSG.2017.2776310.

[16] S. Kar and S. R. Samantaray, "A Fuzzy Rule Base Approach for Intelligent Protection of Microgrids," Electr. Power Components Syst., vol. 43, no. 18, pp. 2082-2093, 2015, doi: 10.1080/15325008.2015.1070384.

[17] F.A.S. Dizioli, P.H.A. Barra, T.S. Menezes, V.A. Lacerda, D.V Coury, and R.A.S. Fernandes, "Multi-agent system-based microgrid protection using angular variation: An embedded approach," Electr. Power Syst. Res., vol. 220, p. 109324, 2023, [Online]. Available: https://doi.org/10.1016/j.epsr.2023.109324.

[18] R. Jain, Y. Nag Velaga, K. Prabakar, M. Baggu, and K. Schneider, "Modern trends in power system protection for distribution grid with high DER penetration," e-Prime - Adv. Electr. Eng. Electron.

Energy, vol. 2022, no. July, pp. 2772-6711, 2022, doi: 10.1016/j.prime.2022.100080.

[19] Y. Seyedi and H. Karimi, "Coordinated Protection and Control Based on Synchrophasor Data Processing in Smart Distribution Networks," IEEE Trans. Power Syst., vol. 33, no. 1, pp. 634-645, 2018, doi: 10.1109/TPWRS.2017.2708662.

[20] P. Kundu and A.K. Pradhan, "Supervisory protection of islanded network using synchrophasor data," IEEE Trans. Smart Grid, vol. 10, no. 2, pp. 1772-1780, 2019, doi: 10.1109/TSG.2017.2777873.

[21] S. Papathanassiou, "Study-Case LV Network," [Online]. Available: http://microgrids.power.ece.ntua.gr/documents/Study-Case%20LV-Network.pdf.